Electronic structure of normal, inverse, and partially inverse spinels in the $MgAl_2O_4$ system

Shang-Di Mo and W. Y. Ching
Department of Physics, University of Missouri–Kansas City, Kansas City, Missouri 64110
(Received 8 July 1996; revised manuscript received 19 August 1996)

The electronic structure of normal, inverse, and partially inverse spinels in the $MgAl_2O_4$ system are studied by means of first-principles calculations. For the normal spinel, the calculated ground-state properties are in good agreement with experimental data. A local-density-approximation band gap of 5.80 eV is obtained. For the inverse and partially inverse spinels, in which up to eight Mg atoms in a tetrahedral coordination are interchanged with eight of the 16 Al atoms in octahedral coordination, the atomic positions are relaxed by realistic interatomic pair potentials. Based on the relaxed models, the electronic structure and their dependence on the inversion parameter λ are studied. The total lattice energy increases as λ increases with a change of slope at $\lambda=\frac{4}{16}$. It is found that the general features in the density of states (DOS) in these spinels are quite similar with subtle differences in the peak structures between normal and inverse spinels. The smallest band gap of 4.84 eV is found at $\lambda=\frac{4}{16}$. The orbital decomposition of the partial DOS of Al and Mg in different coordination environments is fully analyzed. These results are discussed in the context of an order-disorder phenomenon associated with a cation site interchange, and their implications on spectroscopic detections. [S0163-1829(96)05947-4]

I. INTRODUCTION

Spinel oxides or sulfides comprise an important class of ceramic compounds with a variety of interesting electrical, magnetic, and optical properties.[1] Some spinels are superconductors with relatively high transition temperatures.[2] Others have applications as magnetic cores and in geophysics.[3–5] Recently discovered spinel oxides with wide band gaps and high electroconductivity offer promising applications in photoelectronics.[6] In particular, the magnesium spinel ($MgAl_2O_4$) has a combination of desirable properties of high melting point, high strength, resistance to chemical attack, and low electrical losses.[7] These special properties mean that a magnesium spinel has many important applications. Recently, it was reported[8] that a magnesium spinel in porous form may be used as a humidity sensor for monitoring and controlling the humidity of the environment due to its stability.

The spinel has a close-packed face-centered-cubic structure[9] [space group $Fd3m(O_h^7)$], with eight $MgAl_2O_4$ units per cubic cell. (In this paper, a spinel is referred to specifically to $MgAl_2O_4$ unless stated otherwise.) Its crystal structure is characterized by two parameters: the lattice constant a and the oxygen parameter u. In an ideal spinel, the O anions form a cubic sublattice with $u=\frac{3}{8}=0.375$, but for most spinels $u\neq0.375$, which results in a trigonal distortion of the O octahedron along the [111] direction. Two types of spinels can be distinguished; normal and inverse spinels. In the normal spinel, all Al^{3+} ions are in an octahedral coordination with a local symmetry D_{3d}, and all Mg^{2+} ions are in a tetrahedral coordination with a point group symmetry T_d. Thus the general formula may be written as $(Mg)[Al_2]O_4$ or $(Mg_8)[Al_{16}]O_{32}$ for the cubic cell, where ( ) and [ ] denote tetrahedral and octahedral sites, respectively. The Mg-O and Al-O bond lengths in the normal spinel are 1.967 and 1.855 Å, respectively. Figures 1(a) and 1(b) show two sublattice structures of AlO_6 and MgO_4 coordinations in the normal spinel. The inverse spinel can be described by the formula $(Al)[MgAl]O_4$ or $(Al_8)[Mg_8Al_8]O_{32}$. The Mg^{2+} and Al^{3+} ions occupy the octahedral sites in equal proportions. Between these two extremes, there exist intermediate phases with random cation distributions. It is convenient to characterize the partially inverse phases by defining an inversion or disorder parameter λ, which is the fraction of octahedral sites occupied by Mg^{2+}. The structural formula now becomes $(Mg_{1-2\lambda}Al_{2\lambda})[Mg_{2\lambda}Al_{2-2\lambda}]O_4$ or $(Mg_{8-16\lambda}Al_{16\lambda})[Mg_{16\lambda}Al_{16-16\lambda}]O_{32}$. λ ranges from 0 for the normal spinel to 0.5 for the inverse spinel. $\lambda=\frac{1}{3}$ corresponds to a complete random distribution.

While most spinel oxides are normal, inverse spinels are fairly common especially when one of the metal elements is a transition element such as in Fe_3O_4, $NiAl_2O_4$, or $CuAl_2O_4$. The wide range of cation distributions found in spinels is perhaps the most interesting feature of this class of compound. For example, the magnetic and electrical properties of cobalt ferrite ($Co_xFe_{3-x}O_4$) depend strongly on the cation

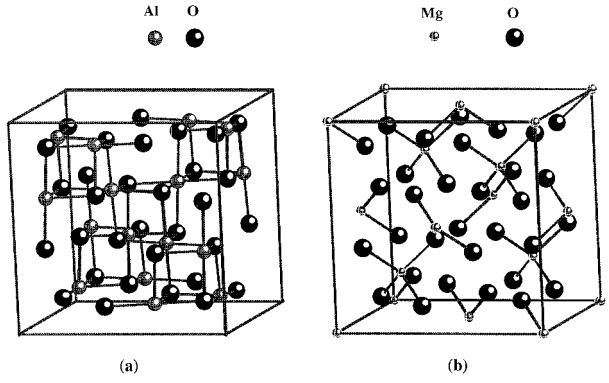

FIG. 1. Crystal structure of a normal $MgAl_2O_4$ spinel showing sublattices for (a) Al-O_6 octahedral coordination, and (b) Mg-O_4 tetrahedral coordination.

of the distribution.[10] More than 60 years ago Barth and Posnjak observed that not all spinel structures could be described by the same cation distribution.[11] Since then, considerable efforts have been put forward to identify and understand the key factors that control this distribution.[12] Hafner,[13] and also Fischer,[14] showed that the $MgAl_2O_4$ spinel may be partially inverse. Wood, Kirkpatrick, and Montez[15] showed that natural $MgAl_2O_4$ has a very small inversion parameter ($\lambda<0.025$). However, to our knowledge, there have been few quantitative studies of inverse and partially inverse spinels, and there are difficulties in understanding their thermochemical and physical properties. This is mainly due to the unquantified extent associated with the cation site exchanges.[15,16] To complicate the matter even further, in the nonstoichiometric spinels $MgO_xAl_2O_3$ with $x>1$, a cation vacancy at the octahedral site may exist.[17] Within the last few years, attempts were made to determine the cation distribution in $MgAl_2O_4$ accurately using analytical techniques. One of them, ^{27}Al magic angle spinning NMR,[18] was used to distinguish between the tetrahedrally and octahedrally coordinated Al sites in spinels with fair accuracy. The electron-spin-resonance technique was also used to study the temperature dependence of λ in $MgAl_2O_4$.[19] Nevertheless, there remain many uncertainties and discrepancies. One intensely studied area in ceramic materials is the structure and properties of the metal-ceramic interface.[20–22] The central issue is to know whether the interface is metal or O terminated, and whether intermediate phases such as a spinel or inverse spinel may exist. A common experimental technique is electron-energy-loss spectroscopy, especially the energy-loss near-edge structure. Such spectroscopic studies of the buried interfaces require a knowledge and understanding of specific bonding of the metal ions in a different coordination environment. It is highly desirable to make a systematic investigation of the structure and properties of spinel systems by theoretical means, especially of the λ dependence of electronic properties of partially inverse spinels. Past theoretical works were limited to classical calculations. Navrotsky and Kleppa[23] calculated the enthalpy change of the disorder and the empirical site preference energies in several spinel oxides, and related them to calorimetric data. Cormack *et al.*[24] carried out detailed calculations on lattice energies in a number of spinels using short-range pair potentials of the Buckingham type. They found that if different pair potential parameters are used to account for different coordinations, the observed cation distributions in many spinels can be correctly predicted. Xu and Ching[25] carried out first-principles calculations of the electronic structure and optical properties of the normal spinel.

In this paper, we report a systematic investigation of the electronic properties of normal, inverse, and partially inverse spinels. The paper is organized as follows: In Sec. II, the computational approaches used are described. In Sec. III, the calculated results are presented and discussed. Some conclusions are given in Sec. IV.

II. COMPUTATIONAL APPROACHES

In the present study, all calculations are confined to a 56-atom cubic cell with a fixed lattice constant. It has been shown that the effect of disorder on the cell edge is extremely small.[15] For ground-state properties of the normal spinel, we use the self-consistent orthogonalized linear combination of atomic orbitals (OLCAO) method.[26] This is a first-principles method based on the density-functional theory within the local-density approximation (LDA).[27] The crystal Bloch functions are linear combinations of atomic orbitals of O($1s$, $2s$, $2p_x$, $2p_y$, $2p_z$, $3s$, $3p_x$, $3p_y$, and $3p_z$), Mg, and Al ($1s$, $2s$, $2p_x$, $2p_y$, $2p_z$, $3s$, $3p_x$, $3p_y$, $3p_z$, $4s$, $4p_x$, $4p_y$, $4p_z$, $3d_{xy}$, $3d_{yz}$, $3d_{x^2-y^2}$, and $3d_{3z^2-r^2}$) which are expanded in terms of Gaussian-type orbitals. The Wigner interpolation formula is used to account for correlation correction.[28] The potential and charge densities are expressed as sums of atom-centered functions which are updated at each iteration. Self-consistency is achieved when the eigenvalues converge to within 0.0001 eV. By fitting the calculated total energy $E_{\rm tot}$ as a function of crystal volume to the Murnaghan equation of states,[29] we obtain the equilibrium volume, the bulk modulus B_0, and the pressure coefficients B_0' for the normal spinel.

TABLE I. Interatomic pair potential parameters used in the present calculation.

Atomic pair	A_{ij} (eV)	ρ_{ij} (Å)	C_{ij} (eV Å^6)
Al-O	1012.6	0.3118	0.0
Mg-O	821.6	0.3242	0.0
O-O	22764.3	0.149	27.88

For the inverse and partially inverse spinels, we use the atomistic modeling technique to account for possible structural changes upon the interchange of Mg and Al ions. It is necessary to relax the atomic positions within the cubic cell for the inverse or partially inverse spinels using a suitable pair-potential function. In this work, we use the pair-potential $V_{ij}(r)$ of the Born-Mayer-Huggins form developed by Wolf, Walker, and Catlow,[30]

$$V_{ij}(r)=Z_iZ_je^2/r+A_{ij}\exp(-r/\rho_{ij})-C_{ij}/r^6,$$

where Z_i is the charge on ions of type i. The three terms on the right side of the equation represent the long-range Coulomb interaction, short-range repulsion, and dispersion energies, respectively. The long-range Coulomb potential is evaluated by Ewald summation.[31] The spinels are assumed to be fully ionic with formal charges of $Z_i=+2$, $+3$ and -2 for Mg, Al and O, respectively. The parameters A_{ij}, ρ_{ij}, and C_{ij} for the different ion pairs are derived empirically, so as to reproduce the lattice structure of the normal spinel. They are listed in Table I. We obtained the equilibrium lattice parameters of $a=7.9462$ Å and $u=0.387$, which differ from the experimental data by only -1.7% and $+1.5\%$, respectively. We thus consider these pair potentials to be adequate for structural relaxation of the inverse and partially inverse spinels.

It is clear that for each λ of the partially inverse spinels, there can be many nonequivalent lattice configurations with different total energies. In other words, the possibilities of site exchange between tetrahedral Mg^{2+} and octahedral Al^{3+} are not unique for each λ. Our strategy is to deal with as many configurations as practical, and take the average value as the mean energy value for that λ. We then choose a lattice

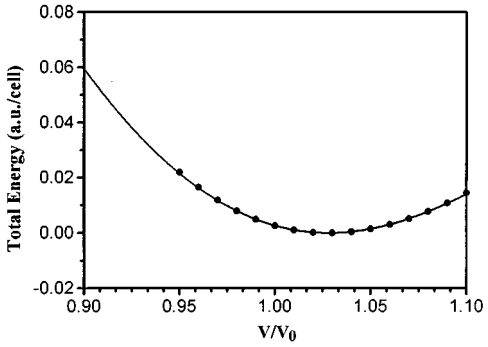

FIG. 2. Calculated total LDA energy of the normal spinel as a function of crystal volume.

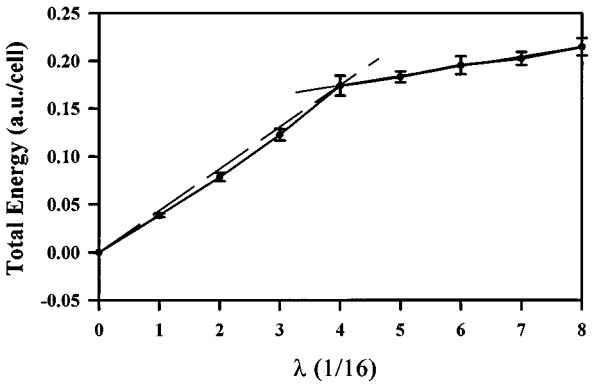

FIG. 3. λ dependence of the interaction energy calculated after pair-potential relaxation. ($\lambda=0$ and $\frac{8}{16}$ correspond to normal and inverse spinels, respectively). Error bars indicate the rms, derivation over several configurations. Dashed and solid lines indicate the different slopes for λ below and above $\frac{4}{16}$.

configuration with the total interaction energy closest to the average value for each λ, and perform self-consistent electronic structure calculation on the relaxed models. After self-consistency in the potential has been obtained, the eigenvalues and eigenvectors of the band secular equation are solved at 56 k points in the $\frac{1}{8}$th portion of the Brillouin zone. The energies and wave functions at these k points are used to evaluate the density of state (DOS) using the linear analytic tetrahedron method.[32] The site and orbital resolved partial components (PDOS) are obtained by Mulliken analysis.[33] The λ dependence of the electronic properties can then be analyzed.

III. RESULTS AND DISCUSSIONS

A. Ground-state properties of normal $MgAl_2O_4$ spinel

Figure 2 shows the calculated total LDA energy E_{tot} as a function of crystal volume for the normal spinel. We have assumed the symmetry of the crystal under pressure to remain the same as in the equilibrium case (i.e., the parameter u is fixed). The minimum in the $E_{\text{tot}}(V)$ curve gives an equilibrium volume in good agreement with the experiment. By fitting the calculated data points to the Murnaghan equation of states,[29] we obtained the bulk modulus B_0 and the pressure coefficient B_0' of the normal spinel to be 2.13 Mbar and 5.40, respectively. Measurement of elastic constants by Yoneda[34] gave an estimated B_0 of the normal spinel to be 1.96 Mbar, and B_0' to be 5.3, in very close agreement with our calculated values. Very recently, Kruger *et al.*[35] obtained B_0 and B_0' values of 1.96 Mbar and 4.7 by quasihydrostatic x-ray-diffraction measurements, which also agree well with the calculated results. These results are summarized in Table II.

TABLE II. Ground-state properties of the normal spinel.

	This work	Expt.
V_{min}/V_0	1.028	1.00
B_0 (Mbar)	2.13	1.96[a], 1.96[b]
B_0'	5.40	5.3[a], 4.7[b]

[a]Reference 34.
[b]Reference 35.

B. Relaxed lattice models and the λ dependence of the total energy

In the normal spinel, each Mg(Al) is coordinated with four (six) O with equal Mg,-O (Al-O) bond lengths of 1.967 Å (1.855 Å). These are highly symmetric regular tetrahedral and octahedral units. After interchange of ions, the symmetry is broken and the Mg-O and Al-O interatomic distances change. We found that upon the exchange of Al and Mg ions in the inverse and partially inverse spinels, the Al-O bond lengths for Al at the octahedral site increase only slightly as a function of λ. The average Al-O bond length for Al at the tetrahedral site is smaller than those at the octahedral sites by about 0.5 Å. For the Mg-O bond lengths, those at the octahedral site are larger than those at the tetrahedral sites by about 0.5 Å. The maximum deviation of bond lengths appears to occur at $\lambda=4/16$.

The λ dependence of the total interaction energy in the cubic cell of the inverse and partially inverse spinels is shown in Fig. 3. The calculated data points are the average values of many nonequivalent lattice configurations, and the ''error bars'' represent the root-mean-square deviations. We found that although the interaction energies for each λ have large variations for nonequivalent configurations before lattice relaxation, those obtained after lattice relaxation are very close, as can be seen by the relatively small error bars in Fig. 3. The largest error bar is at $\lambda=\frac{4}{16}$. This underscores the importance of the structural relaxation process for the inverse and partially inverse spinels. In general, as λ increases, the interaction energy increases. From $\lambda=0$ to $\frac{4}{16}$, the increase is more rapid, with a small bowing of an otherwise linear curve. From $\lambda=\frac{4}{16}$ to $\frac{8}{16}$, the increase is much smaller and is in a strictly linear fashion. This curve implies that for the partially inverse spinels, $\lambda=\frac{4}{16}$ is at the boundary of two rather different disordering processes above and below it. This may be related to the fact that the normal spinel cube consists of eight octants, four of them containing Mg cations in a tetrahedral coordination and four others containing Al cations in an octahedral coordination. Figure 3 is in line with several experimental measurements[15,18] of the temperature dependence of λ in inverse spinels. Although λ increases with T at low temperatures, above $T=900$ °C the curve is

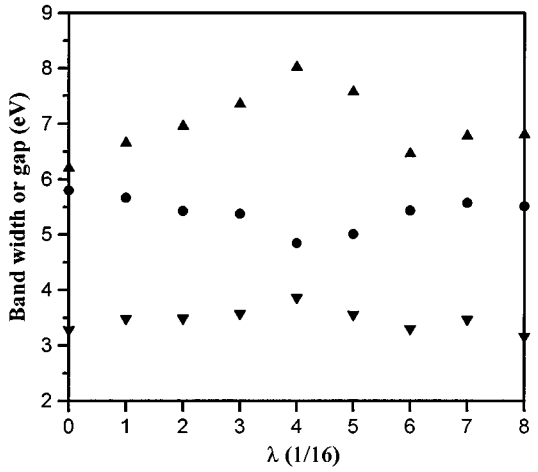

FIG. 4. λ dependence of the band gap (solid circle), bandwidths of upper (up solid triangle) and lower (down solid triangle) VB's.

almost flat, indicating that, for high λ, the relative difference in the configuration energies should be quite small.

C. λ dependencies of electronic properties

Figure 4 shows the λ dependence of the band gap E_g, and the upper and lower valence-band (VB) widths. The normal spinel has a LDA gap of 5.80 eV, which is smaller than the measured gap[36] of 7.8 eV by 25%, and is slightly larger than the band gap of 5.51 eV for the inverse spinel. Previous calculation by Xu and Ching[25] gave a slightly larger gap for the normal spinel. The small difference is attributed to the improved potential and charge-density representation in the present calculation. For partially inverse spinels, the minimum band gap occurs at $\lambda=\frac{4}{16}$ with a value of 4.84 eV. Thus all spinels in the $MgAl_2O_4$ system should be transparent. In general, the energy gap decreases for λ from 0 to $\frac{4}{16}$, and then increases for λ above $\frac{4}{16}$. The widths of the lower and upper VB generally increase for λ from 0 to $\frac{4}{16}$, and decrease for λ above $\frac{4}{16}$. In addition, the maximum widths of the lower and upper VB's occur at $\lambda=\frac{4}{16}$. Although our calculation for the electronic structure for each λ is carried out only for a single configuration rather than averaged over many configurations, still the result seems to suggest that the maximum disorder occurs at $\lambda=\frac{4}{16}$. A calculation of the crystalline and amorphous SiO_2 phases using the same OLCAO method shows that the amorphous phase has a smaller band gap and larger VB widths.[37]

An important aspect of the electronic structures is the DOS of the normal, inverse, and partially inverse spinels. The top panel of Fig. 5 shows the calculated DOS of the normal spinel which is similar to a previous calculation using the same method.[25] The lower O 2*s* band splits into two pieces, a very sharp peak at −15.9 eV and a lower piece 2.0 eV wide with double peaks at −18.3 and −17.7 eV. The upper VB consists mainly of O 2*p* orbitals, and has three well-resolved peaks at −0.80, −2.69, and −4.90 eV. The conduction-band (CB) DOS has multiple structures. Its atomic and orbital origin will be discussed later in the context of the PDOS.

Figure 5 also shows the total DOS of the inverse and partially inverse spinels for $\lambda=\frac{2}{16}$, $\frac{4}{16}$, $\frac{6}{16}$, and $\frac{8}{16}$. Again, the

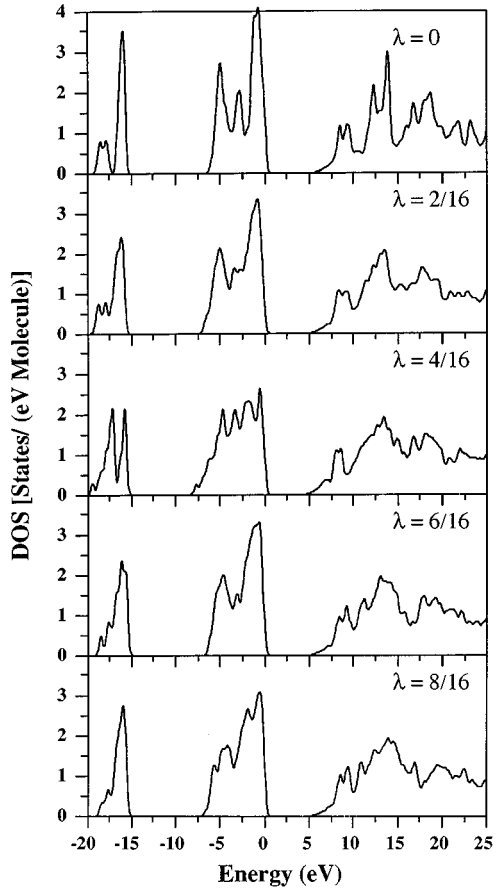

FIG. 5. Total DOS's of the normal spinel (λ=0), partially inverse spinels ($\lambda=\frac{2}{16}$, $\frac{4}{16}$, and $\frac{6}{16}$), and the inverse spinel ($\lambda=\frac{8}{16}$).

calculation is based on a single configuration for each λ. Although the gross features of these DOS diagrams appear to be similar, subtle differences can be identified when λ changes. The top of the VB edge remains sharp. This implies that there are no significant defective states associated with cation exchange and the subsequent lattice relaxation in the inverse and partially inverse spinels. For $\lambda=\frac{4}{16}$, the sharp double-peak structure in the lower VB is quite distinct from the low- or high-λ cases. In the upper VB, the relative strength of the peaks changes as λ changes. For $\lambda=\frac{4}{16}$, four prominent peaks develop instead of the original three. We interpret this as an indication that, at $\lambda=\frac{4}{16}$, there is the greatest disorder associated with the bonding of the interchanged cations. The changes in the CB DOS as λ increases are rather subtle because of the presence of multiple structures. The changes in the relative strengths of different peaks are related to the cation exchange. The total DOS of the inverse spinel ($\lambda=\frac{8}{16}$) is quite different from the normal spinel in peak structures. These differences will be fully elucidated below.

D. Coordination dependencies of the PDOS in the spinel

As discussed in Sec. III C the electronic properties, especially the DOS, is somewhat dependent on λ. It is of interest to trace the origin of such changes. To this end, we investigate the PDOS of Al and Mg in normal and inverse spinels at different sites. Figure 6 shows the PDOS of Al in normal spinel at the octahedral sites. We shall concentrate on a dis-

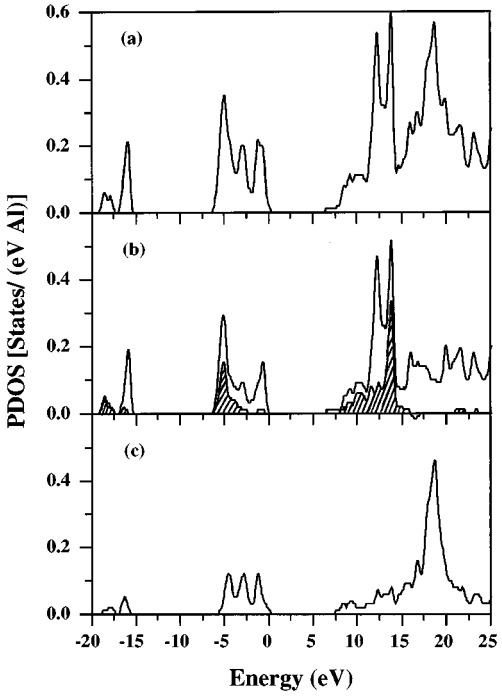

FIG. 6. PDOS of Al in the normal spinel at the octahedral site: (a) total; (b) s and d orbital states with the s portion shaded; (c) p orbital states.

cussion of the CB region. The PDOS is resolved into s $(3s,4s)$, d $(3d)$, and p $(3p,4p)$ orbital components. The s and d parts are added together since they are both of even parity. In many spectroscopic experiments, transitions to states of the same parity cannot be resolved. Roughly speaking, the CB PDOS is characterized by three sharp peaks at 12.3, 14.0, and 19.1 eV, respectively of $3d$, $3s$, and $3p$ origins. Figure 7 shows the Al PDOS at the tetrahedral site in the inverse spinel. As expected, different local coordinations give completely different PDOS spectra. The lowest peak at

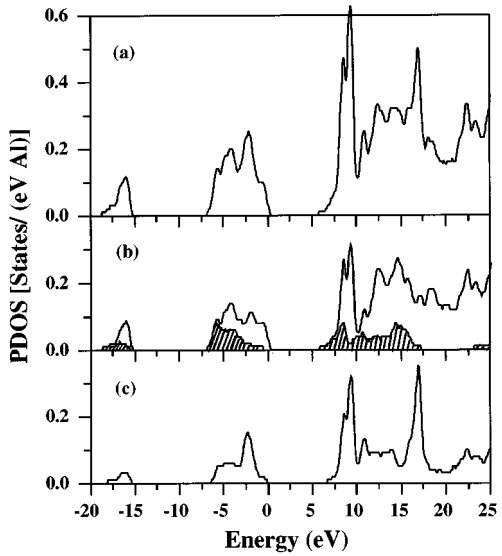

FIG. 7. PDOS of Al in the inverse spinel at the tetrahedral site: (a), (b), and (c) same notation as Fig. 6.

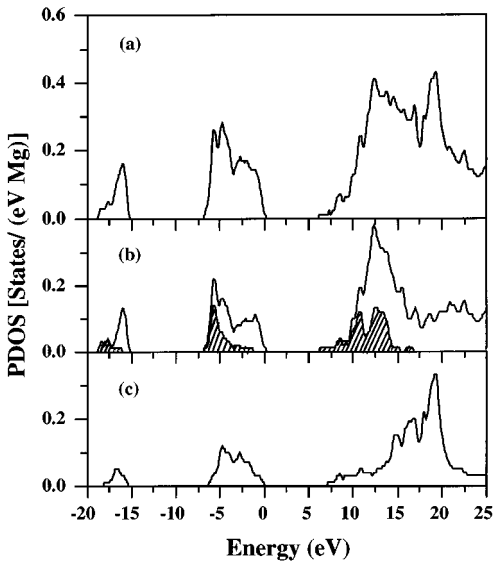

FIG. 8. PDOS of Al in the inverse spinel at the octahedral site: (a), (b), and (c) same notation as Fig. 6.

9.3 eV has its origin from both Al $3d$ and Al $3p$ orbital states. The other sharp peak at 17.4 eV is from Al $3p$. The contribution from Al $3s$ is quite minor. Other structures between the peaks at 9.3 and 17.4 eV are basically from Al $3d$ states. Figure 8 shows the Al PDOS at the octahedral site in the inverse spinel. Comparing with the Al PDOS at the octahedral site in the normal spinel (Fig. 7), we find some nontrivial differences in spite of the same local coordination. The lower two peaks are now merged to give a rather broad peak at 12.7 eV, and the higher Al $3p$ peak is shifted slightly to 19.5 eV, and also becomes broader. These differences reflect the second-nearest-neighbor effects, and cannot be explained by a simple argument based on local coordination alone. They can only be obtained by realistic first-principles calculations.

Figures 9 and 10 show the PDOS of Mg at the tetrahedral site in the normal spinel and at the octahedral site in the inverse spinel, respectively. For the tetrahedral site in the normal spinel, the CB PDOS below 20 eV basically consists of three groups of multiple peaks centered at 9.1, 13.5, and 18 eV. Inspection of their partial components shows that Mg $3s$, Mg $3p$, and Mg $3d$ all contribute to these three groups of major peaks. This is quite different from the Al PDOS at the octahedral sites in the normal spinel. When all the Mg atoms are placed at the octahedral sites in the inverse spinel, the CB PDOS shown in Fig. 10 becomes very different. It essentially reduces to two main peaks. The lower one around 14.0 eV is dominated by Mg $3d$ orbitals, and the higher peak at 20.3 eV is from the Mg $3p$ orbitals. The contribution from Mg $3s$ is basically overshadowed by the Mg $3d$ contribution in the same region. Hence, like the Al PDOS, the increased disorder due to cation exchange in the inverse spinel has resulted in the rather different and more broadened CB PDOS spectra.

The above results can be compared with the Al $L_{2,3}$ and Mg $L_{2,3}$ energy-loss near-edge fine structure in $MgAl_2O_4$ by Bruley, Tseng, and Williams.[38] These spectra measure the transition probability from the isolated $2p$ core levels to the

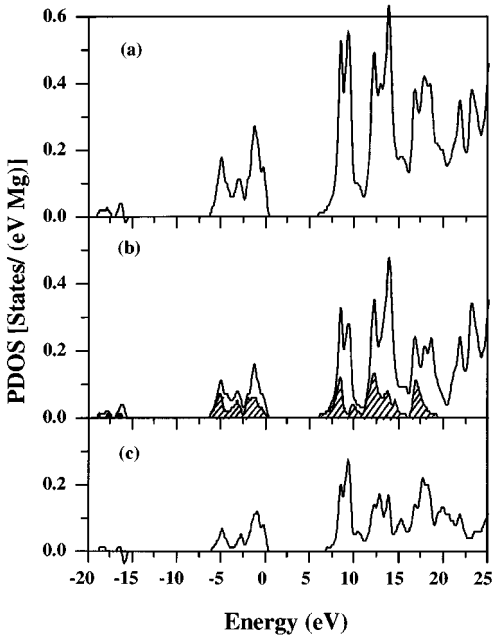

FIG. 9. PDOS of Mg in the normal spinel at the tetrahedral site: (a), (b), and (c) same notation as Fig. 6.

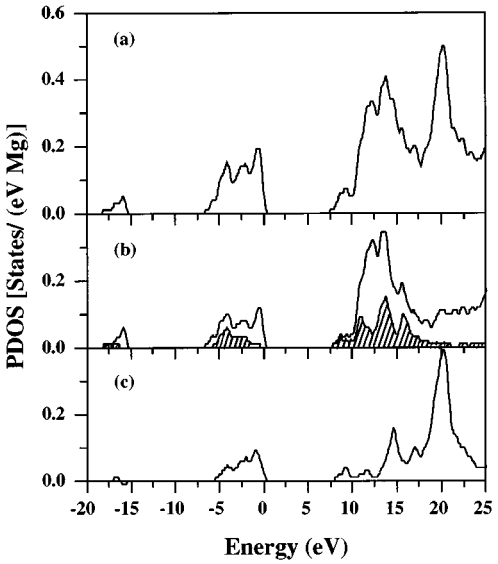

FIG. 10. PDOS of Mg in the inverse spinel at the octahedral site: (a), (b), and (c) same notation as Fig. 6.

3*s* and 3*d* CB states, and can be meaningfully compared with Figs. 6(b) and 9(b). Although the sample in that measurement may not be stoichiometric and the resolution is rather low, the structures within a 10–15-eV region in the experimental curve show a strong resemblance to the calculated PDOS. It is highly desirable that more accurate data on well-characterized samples be made available so that better-focused interpretation can be carried out.

IV. CONCLUSIONS

We have investigated the electronic and structural properties of normal, inverse, and partially inverse spinels by means of first-principles OLCAO calculations. We believe this is the first systematic investigation on the electronic structures of inverse and partially inverse spinels. The calculated ground-state properties for the normal spinel are in good agreement with experiments. The structures of the inverse and partially inverse spinels are modeled by realistic pair potentials, and are shown to have a slightly increased energy over the normal phase. The calculated band gaps show that $\lambda=\frac{4}{16}$ has the smallest band gap, and that the band gap of the inverse spinel is slightly smaller than the normal spinel. The λ dependence of the electronic structure suggests that the maximum disorder occurs at λ close to $\frac{4}{16}$. Analysis of site- and orbital-resolved PDOS's shows a significant dependence of the Al and Mg CB PDOS's on the local coordinations. Even for Al at octahedral sites in normal and inverse spinels, their PDOS's show considerable differences because of the disorder introduced in the inverse spinel due to cation exchange. These results are important for the interpretation of various experiments involving different phases of spinels in the $MgAl_2O_4$ system.

ACKNOWLEDGMENT

This work was supported by U.S. DOE under Grant No. DE-FG02084ER45170.

[1] F. S. Galasso, *Structure and Properties of Inorganic Solids* (Pergamon, New York, 1970)

[2] R. W. McCallum, D. C. Johnston, C. A. Luengo, and M. B. Maples, J. Low. Temp. Phys. **25**, 177 (1976).

[3] W. Schiessl *et al.*, Phys. Rev. B **53**, 9134 (1996).

[4] R. E. Wandenberghe and E. De Grave, in *Mössbauer Spectroscopy Applied to Inorganic Chemistry*, edited by G. J. Long and F. Grandjean (Plenum, New York, 1989), Vol. 3.

[5] K. Wakamura, J. Solid State Chem. **78**, 197 (1989).

[6] N. Ueda, T. Omata, N. Hikuma, K. Ueda, H. Mizoquchi, T. Hashimoto, and H. Kawazoe, Appl. Phys. Lett. **61**, 1954 (1992); T. Omata *et al.*, *ibid.* **62**, 499 (1993); **63**, 3335 (1993); **64**, 1077 (1994).

[7] C. Baudín, R. Martínez, and P. Pena, J. Am. Ceram. Soc. **78**, 1867 (1995).

[8] G. Gusmano, G. Montesperelli, P. Nunziante, and E. Traversa, Br. Ceram. Trans. **92**, 104 (1993).

[9] R. J. Hill, J. R. Graig, and G. V. Gibbs, Phys. Chem. Miner. **4**, 317 (1979).

[10] J. G. Na, T. D. Lee, and S. J. Park, IEEE Trans. Magn. **28**, 2433 (1992).

[11] T. F. W. Barth and E. Posnjak, Z. Kristallogr. **82**, 325 (1932).

[12] See, for example, J. K. Burdett, G. D. Price, and S. L. Price, J. Am. Chem. Soc. **104**, 92 (1982).

[13] S. Hafner, Schweiz. Mineral Petrogr. Mitt. **40**, 207 (1960); S. Hafner, and F. Laves, Z. Kristallogr. **115**, 321 (1961).

[14] P. Fisher, Z. Kristallogr. **124**, 275 (1967).
[15] B. J. Wood, R. J. Kirkpatrick, and B. Montez, Am. Mineral. **71**, 999 (1986).
[16] H. St. C. Óneill and A. Navrotsky, Am. Mineral. **68**, 181 (1983).
[17] R. Dupree, M. H. Lewis, and M. E. Smith, Philos. Mag. A **53**, L17 (1986).
[18] G. C. Gobbi, R. Christoffersen, M. T. Otten, B. Miner, P. R. Buseck, G. J. Kennedy, and C. A. Fyfe, Chem. Lett. Jpn. **1985**, 771.
[19] U. Schmocker and F. Waldner, J. Phys. C **9**, L235 (1976).
[20] F. S. Ohuchi, J. Am. Ceram. Soc. **74**, 1163 (1991).
[21] J. Bruley, R. Brydson, H. Müllejans, J. Mayer, G. Gutekunst, W. Mader, D. Knauss, and M. Rüle, J. Mater. Res. **9**, 2574 (1994).
[22] J. C. Yang, E. Schumann, H. Müllejans, and M. Rüle, J. Phys. D **29**, 1716 (1996).
[23] A. Navrotsky and O. J. Kleppa, J. Inorg. Nucl. Chem. **29**, 2701 (1967).
[24] A. N. Cormack, G. V. Lewis, S. C. Parker, and C. R. A. Catlow, J. Phys. Chem. Solids **49**, 53 (1988).
[25] Y.-N. Xu and W. Y. Ching, Phys. Rev. B **43**, 4461 (1991).
[26] W. Y. Ching, J. Am. Ceram. Soc. **73**, 3135 (1990).
[27] H. Hohenberg and W. Kohn, Phys. Rev. **136**, B864 (1964); W. Kohn and L. J. Sham, *ibid*. **140**, A1133 (1965).
[28] E. Winger, Phys. Rev. **46**, 1002 (1934).
[29] F. D. Murnaghan, Proc. Natl. Acad. Sci. U.S.A. **30**, 244 (1944).
[30] M. L. Wolf, J. R. Walker, and C. R. A. Catlow, Solid State Ionics **13**, 33 (1984).
[31] P. P. Ewald, Ann. Phys. (Leipzig) **64**, 253 (1921).
[32] G. Lehmann and M. Taut, Phys. Status Solidi **54**, 469 (1972).
[33] R. S. Mulliken, J. Am. Chem. Soc. **23**, 1833 (1955).
[34] A. Yoneda, J. Phys. Earth **38**, 19 (1990).
[35] M. B. Kruger, J. H. Nguyen, W. Caldwell, and R. Jeanloz, Phys. Rev. B (to be published).
[36] M. L. Bortz, R. H. French, D. J. Jones, R. V. Kasowski, and F. S. Ohuchi, Phys. Scr. **41**, 4404 (1990); M. L. Boltz and R. H. French, Appl. Phys. Lett. **55**, 1955 (1989).
[37] M. Z. Huang and W. Y. Ching, Phys. Rev. B **54**, 5299 (1996).
[38] J. Bruley, M. W. Tseng, and D. B. Williams, Microsc. Microanal. Microstruct. **6**, 1 (1995).